

# Phase-Sensitive Second Harmonic Microscopy Reveals Bipolar Twinning of Markov-Type Molecular Crystals

Peter Rechsteiner,<sup>†</sup> Jürg Hulliger,<sup>\*,†</sup> and Mathias Flörshheimer<sup>‡</sup>

Department of Chemistry and Biochemistry, University of Berne, Freiestrasse 3, CH-3012 Berne, Switzerland, and Physical Institute, University of Münster, Wilhelm-Klemm-Strasse 10, D-48149 Münster, Germany

Received February 17, 2000. Revised Manuscript Received August 28, 2000

Phase-sensitive second harmonic microscopy (PS-SHGM) opens up the possibility of imaging the bipolar state of Markov-type organic supramolecular crystals. During the cocrystallization of dipolar guest and nonpolar host compounds, channel-type inclusion compounds form crystals composed of adjacent macrodomains featuring opposite polarities. Through a comparison with crystals of known absolute polarity, the application of PS-SHGM allows a fast noncontact mapping of the domain structure and a determination of the absolute polarity of thin organic and other nonlinear optical crystals.

## Introduction

The characterization of polar supramolecular materials with designer properties is a fundamental target of contemporary materials research. Markov-type molecular crystals are materials for which the polarity at the macroscopic level originates from a stochastic process of molecular ordering during the process of crystal growth.<sup>1,2</sup> Real examples are channel-type inclusion compounds formed by particular host and linearly shaped dipolar guest molecules [host, e.g., perhydrotriphenylene (PHTP) or 1,8-bis((1)-adamantyl)-1,3,5,7-octatetrayne (BAOT)];<sup>3</sup> guest, AD-type molecules where A and D are acceptor and donor substituents, respectively, attached to  $\pi$ -conjugated frameworks]. Polar order is possible if guest molecules assemble into chains within the nanopores of these inclusion compounds (Figure 1). In PHTP, all of the chains of the guest molecules are aligned parallel to each other and are well separated by the saturated hydrocarbon host molecules. Because of the lack of strong lateral interactions between dipolar molecules in different channels, the alignment in the single channels is driven in this case by only short-range interactions between functional groups at the crystal–nutrient interface. In principle, this stochastic mechanism can be applied to all molecular crystals built from achiral dipolar compounds.<sup>4,5</sup>

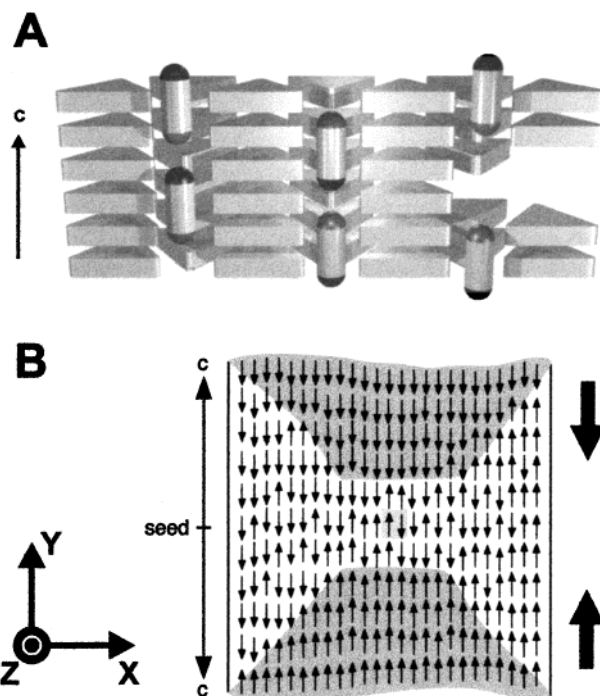


**Figure 1.** (A) Schematic representation of the growth of PHTP host–guest (triangles–pills) crystals: interactions between acceptor (A) and donor (D) terminal groups [dark (A) and bright (D) cappings of the pills] control the alignment of guests during growth along channels. (B) Two-dimensional representation of a bulk crystal. For slowly growing crystals, lateral growth of new channels starts at a random location, resulting in a crystal structured into two cone-like macrodomains of opposing net polarity (shaded regions). The arrows  $\leftarrow$  refer to the molecular dipole moment,  $D \leftarrow A$ . Here, for simplification, the PHTP molecules are omitted. The arrows to the right side show the orientation of the polar vector of a domain. The arrows (x, y, z) indicate the laboratory coordinate system (see Figure 2).

\* To whom correspondence should be addressed. E-mail: juerg.hulliger@iac.unibe.ch.

<sup>†</sup> University of Berne.

<sup>‡</sup> University of Münster.

(1) Hulliger, J.; Rogin, P.; Quintel, A.; Rechsteiner, P.; König, O.; Wübberhorst, M. *Adv. Mater.* **1997**, *9*, 677.

(2) Roth, S. W.; Langley, P. J.; Quintel, A.; Wübberhorst, M.; Rechsteiner, P.; Rogin, P.; König, O.; Hulliger, J. *Adv. Mater.* **1998**, *10*, 1543.

(3) Müller, T.; Hulliger, J.; Seichter, W.; Weber, E.; Weber, T.; Wübberhorst, M. *Chem. Eur. J.* **2000**, *6*, 54.

(4) Hulliger, J. *Z. Kristallogr.* **1999**, *214*, 9.

(5) Hulliger, J. *Z. Kristallogr.* **1998**, *213*, 441.

(6) Quintel, A.; Hulliger, J.; Wübberhorst, M. *J. Phys. Chem. B* **1998**, *102*, 4277.

(7) Quintel, A.; Roth, S. W.; Hulliger, J.; Wübberhorst, M. *Mol. Cryst. Liq. Cryst.* **2000**, *338*, 243.

(8) Klap, G. J.; Wübberhorst, M.; Jansen, J. C.; van Koningsveld, H.; van Bekkum, H.; van Turnhout, J. *Chem. Mater.* **1999**, *11*, 3497.

(9) Kurimura, S.; Uesu, Y. *J. Appl. Phys.* **1997**, *18*, 369.

(10) Uesu, Y. *J. Korean Phys. Soc.* **1998**, *32*, S461.

crystals of size 1–3 mm in length and 0.2–0.5 mm in thickness have been investigated.<sup>6,7</sup> The SPEM technique also allows a tomographic view by layerwise thinning of crystals<sup>7</sup> and has currently achieved a lateral resolution of about 2.5  $\mu\text{m}$ , averaging over a surface layer thickness of  $\sim 10 \mu\text{m}$ .<sup>8</sup> For an overview of conventional domain observation techniques for inorganic crystals, see ref 21.

All-optical techniques that enable us to visualize 180° domains are of relevance, for example, for the fabrication of quasi-phase-matched frequency-doubling devices. In this respect, far-field second harmonic microscopy (SHGM) has demonstrated its effectiveness as a non-contact probing technique for the characterization of ferroelectric bulk materials.<sup>9,10</sup> Using the principle of phase-sensitive second harmonic microscopy (PS-SHGM), the possibilities for imaging 180° twinning in thin organic single crystals can now be realized. So far, phase-sensitive second harmonic experiments have been used for the determination of the absolute orientation of molecules at surfaces or interfaces.<sup>11–15</sup>

## Experimental Section

**Synthesis.** For the analysis of the bipolar structure of Markov-type crystals, we have used two congruently melting inclusion compounds, namely PHTP-DMNA (DMNA, 4-nitro-*N,N*-dimethylaniline) and PHTP-NPP [NPP, 1-(4-nitrophenyl)-piperazine]. Thin layer crystals were obtained (i) from a melt placed between glass plates to provide a uniform thickness of a few micrometers and (ii) by solvent evaporation on a glass substrate.

**Sample Preparation.** Thin crystals were prepared from the melt of solid mixtures of the precursors providing molar ratios of PHTP:DMNA = 6.5:1 and PHTP:NPP = 5:1. The materials were crystallized in a press between two silanized glass plates ( $\sim 1 \times 1 \text{ cm}^2$ ). Cooling rates close to the melting temperature were 3.4 K/min. One glass plate was removed before SHG measurements.

2-Butanone was used for solvent evaporation on a single glass substrate for PHTP-NPP crystals (molar ratio  $\approx 8:1$ ).

**Characterization.** For a detailed characterization of solution-grown crystals of PHTP-NPP (structure from X-ray diffraction analysis, crystal growth, and physical properties), see ref 16.

The thickness  $\delta$  of grown layers and its variation  $\Delta\delta$  were measured by AFM and by polarized light microscopy. A layer thickness below the coherence length  $l_c$  (for a definition, see the next section) was confirmed by Maker fringe experiments.<sup>17</sup>

(11) Kemnitz, K.; Bhattacharyya, K.; Hicks, J. M.; Pinto, G. R.; Eisenthal, K. B.; Heinz, T. F. *Chem. Phys. Lett.* **1986**, *131*, 285.

(12) Eisert, F.; Dannenberger, O.; Buck, M. *Phys. Rev. B* **1998**, *58*, 10860.

(13) Corn, R. M.; Higgins, D. A. *Chem. Rev.* **1994**, *94*, 107.

(14) Huang, J. Y.; Lewis, A. *Biophys. J.* **1989**, *55*, 835.

(15) Sato, O.; Baba, R.; Hashimoto, K.; Fujishima, A. *Jpn. J. Appl. Phys.* **1993**, *32*, 1201.

(16) König, O.; Bürgi, H.-B.; Armbruster, T.; Hulliger, J.; Weber, T. *J. Am. Chem. Soc.* **1997**, *119*, 10632.

(17) Jerphagnon, J.; Kurtz, S. K. *J. Appl. Phys.* **1970**, *41*, 1667.

(18) Stolle, R.; Marowsky, G.; Schwarzbarg, E.; Berkovic, G. *Appl. Phys. B* **1996**, *63*, 491.

(19) Nalwa, H. S.; Watanabe, T.; Miyata, S. *Nonlinear Optics of Organic Molecules and Polymers*; Nalwa, H. S., Miyata, S., Eds.; CRC Press: Boca Raton, FL, 1997.

(20) Quintel, A.; Hulliger, J. *Chem. Phys. Lett.* **1999**, *312*, 567.

(21) Kahmann, F.; Matull, R.; Rupp, R. A.; Seglins, J. *Phase Transitions* **1992**, *40*, 171.

(22) Hulliger, J.; Langley, P. J.; Quintel, A.; Rechsteiner, P.; Roth, S. W. *Supramolecular Engineering of Synthetic Metallic Materials: Conductors and Magnets*; Veciana, J., Rovira, C., Amabilino, D. B., Eds.; NATO ASI Series C518; Kluwer Academic Publishers: Dordrecht, The Netherlands, 1999, p 67.

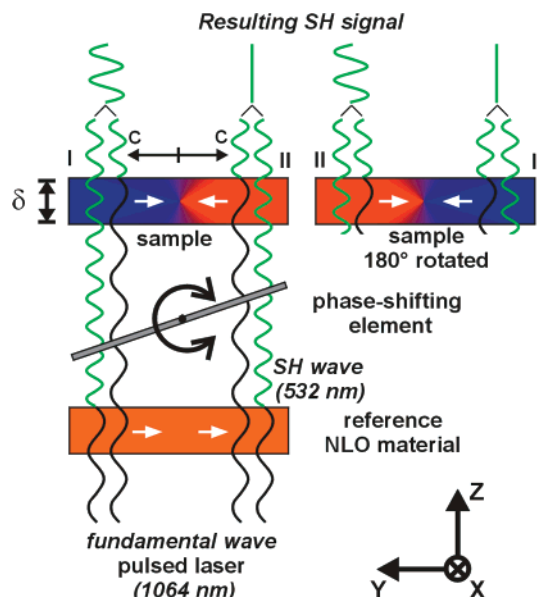


**Figure 2.** Schematic principle of far-field phase-sensitive SH microscopy (PS-SHGM). Oppositely orientated domains (colored blue and red) in a sample with a uniform thickness  $\delta$  emit SH light with a phase shift of  $\pi$ . Domain contrast is achieved by using the interference effect between the sample and a homogeneous SHG reference plate (the white arrows refer to the polarity direction). An angle-tuned glass plate allows for the phase between the (polarized) fundamental waves and the SH waves from the reference plate to be shifted in order to reach maximum intensity, e.g., at the “blue” side of the sample. Keeping optical settings constant and rotating the sample by 180° leads to the opposite contrast: maximum intensity at the “red” side. The arrows ( $x$ ,  $y$ ,  $z$ ) indicate the laboratory coordinate system.

**SHG Microscopy.** For a scheme of the optical geometry, see Figure 2. To visualize polar structures by SHG microscopy and to obtain a maximum SHG intensity, the channel directions in the domains must be oriented parallel to the polarization of the fundamental light. A Leica polarizing microscope (DM RXP, Leitz) was used in transmitted-light mode to allow for background illumination of the samples. A Q-switched Nd:YAG laser (Surelite I-10, Continuum) providing a repetition rate of 10 Hz, a pulse width of 20–25 ns and a pulse energy of  $\sim 25 \text{ mJ}$  ( $\lambda_w = 1064 \text{ nm}$ , pulse intensity  $\approx 10 \text{ MW/cm}^2$ , beam diameter  $\approx 2 \text{ mm}$ ) served for SHG. The unfocused fundamental beam transmitted the samples. An IR absorption filter (KG5, Schott) was used under the objective lens for protection from thermal damage. For 20 $\times$  magnification (Figure 3C), an objective with a long working distance was used (LMPLFL 20 $\times$ , Olympus). Color pictures were taken by a 3CCD color video camera (DXC-950P, Sony) with an electronic shutter for long time exposure. No further image processing was applied.

**Phase-Sensitive SHG.** There are several possible techniques for imparting a controllable phase shift through nonlinear interferometry.<sup>18</sup> The SH reference beam was generated by an angle-tuned  $\text{KH}_2\text{PO}_4$  single crystal (KDP) placed into the fundamental beam. The phase delay between the fundamental and the SH reference beam was adjusted by rotation of a quartz glass plate placed between the KDP crystal (kept at a constant distance from the sample) and the inclusion crystals.

The thickness variations of, e.g., different glass substrates cause an additional phase shift between the fundamental laser beam and the nonlinear optical signal of the reference plate. Therefore, all samples were oriented toward the reference plate. Note that a variation in thickness of about 10  $\mu\text{m}$  can cause a contrast inversion (see next section).

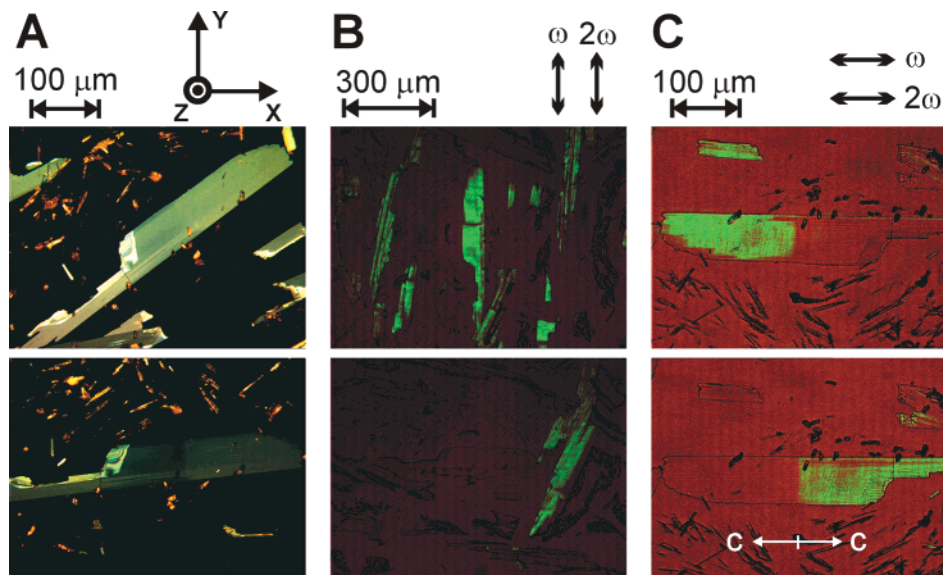


**Figure 3.** Optical characterization (transmitted light mode) of one PHTP-DMNA single crystal obtained from the melt. The crystals belong to an axial point group. (A) Linear optical image (polychromatic, between crossed polarizers) at bright position (upper picture) and at nearly dark (extinction) position (lower picture). (B) Conventional SHG experiment. The dependence of the SH intensity on the polarization of the fundamental light is clearly visible (lower picture, sample rotated by 90°). (C) Domain contrast: visualization of 180° domains. In the upper picture, the SH intensity of one domain is enhanced, while it is attenuated in the other. Contrast inversion occurs if the sample is rotated by 180° (see Figure 2). The lower picture (for comparison rotated by 180° with respect to the upper one) shows the opposite sign of the polarity of the other domain. Some thickness variation is apparent. B and C represent a superposition of the linear optical image and the SH response (green). In these experiments, the fundamental ( $\omega$ ) and the generated ( $2\omega$ ) SH light are polarized along crystal  $c$  axis (indicated by arrows) corresponding to the (+ or -)  $d_{\text{eff}}$  element of the second-order polarizability tensor (except for B, lower picture).

### Results and Discussion

**Theory.** PS-SHGM relies on the fact that the *sign* of the effective nonlinear optical (NLO) coefficient  $d_{\text{eff}}$  is different for macrodomains that are symmetry related by inversion (Figures 1B and 2). When the second harmonic (SH) radiation arises from the electric-dipole response of aligned molecules in PHTP channels,  $d_{\text{eff}}$  is proportional to the sum over the molecular main hyperpolarizability ( $\beta_{i,zzz}$ ).

$$d_{\text{eff}} \propto \sum_i \beta_{i,zzz} \quad (1)$$

When adjacent domains are considered, a change in the sign of  $d_{\text{eff}}$  is related to a phase shift of  $\pi$  for SH waves emerging from either of the domains. Domain mapping is achieved by using the interference effect between the SH waves from a sample and those from a single-domain SHG reference material. Interference between SH waves converts the phase information into a two-dimensional SH image contrast (Figure 2).

Interpretation of a domain mapping becomes simple if the layer thickness  $\delta$  is homogeneous and in the range of or below the coherence length  $l_c$ . The parameter  $l_c$  describes the degree of phase mismatching between the fundamental and the generated SH wave (within a sample) and is defined as

$$l_c = \frac{\lambda_\omega}{4|n_\omega - n_{2\omega}|} \quad (2)$$

where  $\lambda_\omega$  the fundamental wavelength in a vacuum and  $n_{2\omega}$  and  $n_\omega$  are the refractive indices of SH light and fundamental light, respectively.<sup>19</sup> From data on the

refractive index of different NLO organic bulk crystals,<sup>19</sup> we have estimated a lower limit for  $l_c$  of 2–3  $\mu\text{m}$  ( $\lambda_\omega = 1064 \text{ nm}$ ).

Provided that the crystal thickness  $\delta$  is in the range of or below the coherence length  $l_c$ , a reference beam of polarized SH waves is able to undergo constructive or destructive interference with frequency-doubled waves generated within the sample (Figure 2). By adjusting the phase difference between the fundamental and the SH reference waves, all parts of the crystal with the corresponding sign of  $d_{\text{eff}}$  allowing for constructive interference will appear bright, whereas the adjacent macrodomain will release a SH signal of much lower intensity. Keeping optical settings constant but rotating the thin layer crystal around an angle of 180° interchanges the brightness of the macrodomains where either enhanced or attenuated SH waves are generated (Figure 2). Examples of measurements are given by the Figures 3C and 4.

**Analysis of the Bipolar Structure.** Figure 3 shows a qualitative analysis of one typical single crystal of PHTP-DMNA obtained by melt and observed with different positions and magnifications. The crystal shows a thickness  $\delta \approx 1 \mu\text{m}$  and a thickness variation on the surface  $\Delta\delta$  of less than 0.2  $\mu\text{m}$ . Linear optical investigations between crossed polarizers (transmitted light, polychromatic) show a homogeneous interference color for diagonal positions (45°), indicating a uniform thickness and/or birefringence and a uniform extinction for normal positions (0° and 90°, Figure 3A). An SHGM experiment confirms that the NLO response is strongest for a polarization of the fundamental beam parallel to the channel axis (Figure 3B), i.e., the charge-transfer direction of guest molecules corresponding to  $\beta_{zzz}$ . Finally, Figure 3C reveals the bipolar state of the



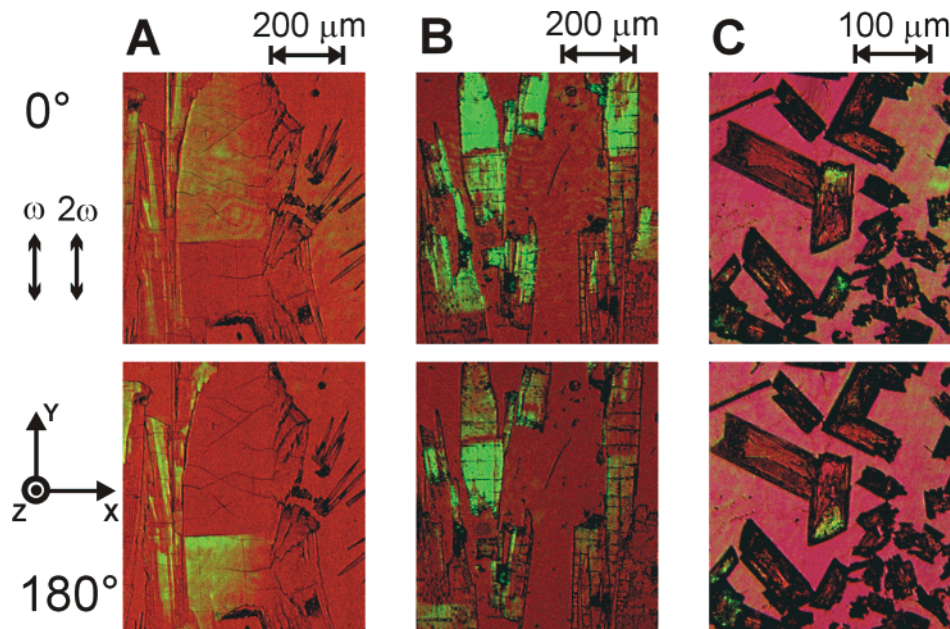


**Figure 4.** PS-SHGM (transmitted light): determination of the absolute but unknown orientation of the polarity of crystals featuring an unrevealed domain structure through comparison with a crystal of well-known absolute polarity. The pictures represent a superposition of the linear optical image and the SH response (green). For clarity, lower pictures are rotated by  $180^\circ$ . The polarization of the fundamental and the SH light is indicated by arrows. (A) PHTP-NPP single crystal obtained from the melt. Here, the crystal was used as a reference sample for which the SHG contrast was optimized (thickness  $\approx 1 \mu\text{m}$ ). For B and C, the optical settings were kept constant. (B) PHTP-DMNA crystals grown from the melt (thickness  $\approx 1 \mu\text{m}$ ). (C) PHTP-NPP crystals grown from solution (thickness  $\approx 2 \mu\text{m}$ ).

supramolecular material as made visible by PS-SHGM. A crystallization event gives rise to both the bright green and the “dark” parts of the crystal when it is simultaneously illuminated by a polarized pulsed laser ( $\lambda_w = 1064 \text{ nm}$ ) and by a reference SH beam adjusted to the SH intensity of the sample. A  $180^\circ$  rotation of the glass substrate (so that it is placed perpendicular to the beam direction) resulted in an interchange of bright and dark parts. Note that some variations  $\Delta\delta$  of the thickness  $\delta$  ( $< l_c$ ) of the crystal cannot be made responsible for the interchange of bright and dark areas, because the interchange of the intensities of SHG responses would not occur when the crystal was rotated around  $180^\circ$ .

As predicted by the Markov model,<sup>1,2,22</sup> the most probable real structure of a solution-grown polar inclusion crystal of, e.g., PHTP-NPP is in agreement with the SPEM results.<sup>6,7</sup> Taking into account both longitudinal and lateral growth, stochastic modeling shows that a nonpolar seed develops into a crystal featuring two conically shaped, polar macrodomains arranged in an opposing fashion, with the seed at their common apex (Figure 1).<sup>2,7</sup> The lateral sections are highly disordered and therefore do not generate SH light. Crystals featuring such cone-shaped domains have been obtained by solution and vapor growth and were measured by SPEM.<sup>6</sup>

A different morphology was observed for the growth from the melt. It seems that the nucleation process for a melt between two silanised glass plates starts from a line (see Figures 3B, C and 4A, B) and not from a pointlike seed as observed in solution- or vapor-grown crystals. Because of constraints on crystal growth between the plates, many crystals grew at nearly constant width. Therefore, we do not expect to observe a cone-shaped evolution of polar domain areas here.<sup>1,2,7</sup>

When realistic energies for the collinear interactions of functional groups along chains of DMNA molecules are assumed, only a few attachment steps along the growth direction are necessary to reach a constant average polarity.<sup>20</sup> This is in agreement with the observed, rather constant SHG intensity seen for both the right and the left side of the seeding part (Figure 3C).

**Determination of the Absolute Polarity.** To determine the absolute polarity of PHTP-DMNA crystals obtained from the melt, we have compared PS-SHGM results of PHTP-DMNA crystals with corresponding responses of PHTP-NPP crystals, a material for which the absolute polarity is known from SPEM results.<sup>6,7</sup> In PHTP-NPP crystals,  $\text{O}_2\text{N}-$  groups (A) of NPP molecules are oriented toward the growing interface. If the absolute polarity of a crystal, i.e., the orientation of the polar vector of a domain, is known, then the attribution of the dipole orientation within other materials when measured at layer thicknesses  $\delta$  below  $l_c$  is allowed. Comparing PS-SHGM results summarized in Figure 4, we can demonstrate that PHTP-DMNA and PHTP-NPP single-crystals feature the same absolute polarity. Because of the predominantly repulsive interaction of the collinear  $-\text{NO}_2 \cdots \text{O}_2\text{N}-$  motif ( $\text{D} \leftarrow \text{A} \cdots \text{A} \rightarrow \text{D}$ , where  $\cdots$  refers to the intermolecular interaction and the arrows refer to the molecular dipole moment) in both DMNA and NPP guest molecules, the Markov model says that, in PHTP inclusion compounds,  $\text{O}_2\text{N}-$  groups are preferably oriented toward the growing interface (Figure 1).<sup>1,2</sup>

Of particular interest are initial experiments in which we have grown thin PHTP-NPP crystals from solution (Figure 4C). This is because, for supramolecular materials, melt growth may often not be possible.

The lateral resolution limit of the stigmatic (nonscanning) microscope is Abbe's limit of the (coherent) SH light, which leads to a theoretical limit of  $0.53 \mu\text{m}$  (for  $\lambda_{2\omega} = 532 \text{ nm}$  and  $\text{NA} = 1$ , where NA is the numerical aperture). At present, the resolution in our setup is limited by the CCD pixel size.

### Conclusions

The present procedure using PS-SHGM opens up the possibility of imaging  $180^\circ$  twinning in *polar organic crystals* grown into sufficiently thin platelets. It allows a fast two-dimensional mapping of polar properties with optical resolution in a nondestructive way. In normal X-ray diffraction or polarized light microscopy, the inclusion compounds would appear as single crystals.<sup>16</sup>

The PS-SHGM investigation of polar supramolecular materials is of interest because an X-ray analysis often encounters difficulties in retrieving a polar domain structure.

The orientational disorder of dipolar components in molecular crystals can lead to spontaneous formation of polar domains.<sup>4,5</sup> A summary of the theoretical concept covering the spontaneous formation of polarity in crystals grown by assembling dipolar components is reviewed elsewhere.<sup>22</sup>

**Acknowledgment.** We thank the Swiss National Science Foundation and the "Stipendienfonds der Basler Chemischen Industrie" for financial support.

CM001018B